Owens Valley and Deep Springs RFI Survey

Marin Anderson and Michael Eastwood
Astronomy Department, California Institute of Technology, Pasadena, CA 91125
mmanders@astro.caltech.edu, mweastwood@astro.caltech.edu

Fig. 1.— The experiment deployed at OVRO near the LWA's third outrigger antenna.

Fig. 2.— The experiment deployed on the Deep Springs valley floor.

1. Introduction

The Cosmic Dawn Array (CDA) is an under-development successor to the Long Wavelength Array (LWA) located at the Owens Valley Radio Observatory (OVRO). Due to its isolation and surrounding mountains, Deep Springs valley is being considered (among other valleys) as a potential site for the CDA. However, the RFI environment of Deep Springs relative to OVRO had not yet been characterized. We present measurements made from an RFI survey conducted over August 14 to 16, 2013 that characterize the RFI environment at OVRO and Deep Springs.

2. Instrumental Setup

The setup for this experiment consisted of:

- LWA antenna (with a shortened OZ post that was manually pounded into the ground)
- LWA active front end
- LWA ground screen
- RF-shielded solar power system – provided by Judd Bowman
  - Weather-proof enclosure
  - RFI cage inside the enclosure
  - Two 125 W solar panels
  - Four 12 V car batteries
  - Charge controller
- Inverter inside its own RFI-tight box – provided by Sandy Weinreb
- Power supply and bias tee for powering the front end
- Rigol DSA815 spectrum analyzer
- Laptop connected via USB cable to the spectrum analyzer

A block diagram of the setup is shown in Fig. 3.

There is some concern that the RFI cage inside the weather-proof enclosure was not actually RFI-tight. In particular, the top of the cage was only

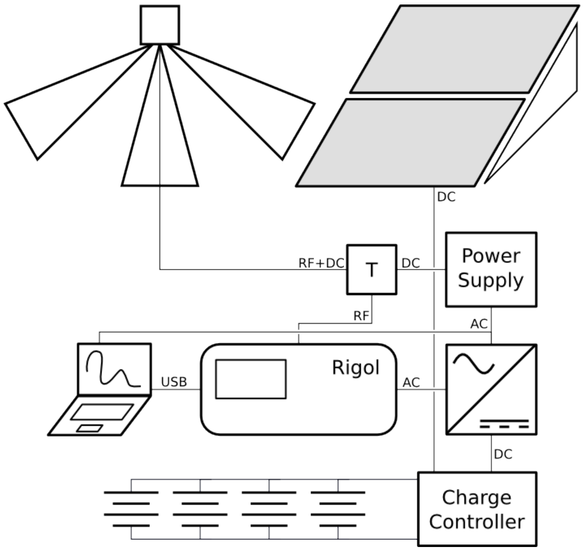

Fig. 3.— A block diagram of the instrumental setup. Everything except the antenna (the front end is mounted on top of the antenna) and solar panel are located inside the weather proof enclosure.

RBW	30 kHz
VBW	30 kHz
Preamp	Enabled
Input Attenuation	10 dB / 0 dB
Averages	~ 10
Detector Type	RMS

Table 1: Rigol DSA815 spectrum analyzer settings.

secured with 4 bolts, and we dropped the nuts to some of these bolts while we were in Deep Springs. Despite the RFI shielding, it is therefore possible some of our results are contaminated with self-generated RFI.

Additionally, the solar power setup was misbehaving such that we suffered occasional power cycles when the charge controller was set to use power from the solar panels. All of the science data was acquired with the solar panels switched off at the charge controller. The charge on the batteries was sufficient for overnight operation.

The spectrum analyzer settings are summarized in Table 1. A laptop was used to run a control script on the spectrum analyzer, which applied these settings. This control script also grabs traces

Fig. 4.— The "neatly" arranged electronic equipment inside the RFI cage. The wiring is summarized in Fig. 3.

from the spectrum analyzer as quickly as it can for a specified period of time.

The resolution of the spectrum analyzer was set to match LEDA's 24 kHz channel size. However, a single spectrum analyzer trace contains only 601 points, which means we could not get channels with 30 kHz spacing if we measured the entire 10 to 100 MHz frequency range at once. Therefore we decided to create 5 frequency bands (10 to 28 MHz, 28 to 46 MHz, 46 to 64 MHz, 64 to 82 MHz, and 82 to 100 MHz). This allows us to get sufficient resolution from the spectrum analyzer's output, but means each frequency band cannot be observed simultaneously. The control script grabbed 100 traces from each frequency band before switching to a new one. Because of this, any one frequency band was only observed a fifth of the time.

Additionally, in testing the control script we discovered that it takes about 0.2 seconds to read a trace from the spectrum analyzer. However, a single sweep of the spectrum analyzer was completed in ~ 0.02 seconds. In order to mitigate this dead time, each trace grabbed by the control script was set to be the average of ~ 10 traces.

3. Results

The results of this experiment are essentially summarized in Figures 6, 7, and 8. In general, all of the plots indicate that Deep Springs is a cleaner site than OVRO. In particular, the total power in the median spectrum (from 10 to 100 MHz) is -20.3 dBm at OVRO, and -47.4 dBm at Deep Springs. This difference is primarily a result of the FM band being ∼30 dB brighter at OVRO than in Deep Springs.

An attempt was made at using kurtosis for automated RFI flagging in order to estimate the occupation of RFI in each channel. However, the use of a spectrum analyzer is not ideal. This is because the raw spectrum analyzer data doesn't take enough samples to rapidly make a good estimate of the kurtosis. A repeated RFI experiment using an ADC and F-engine may be necessary to estimate the occupation of the RFI.

4. LEDA Results

Danny Price (Harvard, CfA) conducted a similar RFI experiment using the LEDA correlator. We were given access to a ∼18 hour span of data with 6 kHz frequency resolution for a single dipole's autocorrelation. This data has a known source of periodic RFI (which the LA DWP has been asked to turn off?). This was excised using a simple total power threshold to flag the corrupted data. After excision, the data was reduced in the same manner as before, and the analogous plots are shown in Figure 9.

5. A Brief Note on the Ionosphere

In low-frequency radio astronomy there is an understanding that waves cannot propagate in a plasma below the plasma frequency ω_p. When a light wave with $\omega < \omega_p$ hits the plasma, the energy contained in the wave cannot propagate through the plasma (and it must go somewhere), so it reflects. However, what is not as well appreciated is the fact that waves with $\omega > \omega_p$ can reflect as well. The goal of this section is to produce a brief quantitative treatment of these reflections to explain the RFI environment in Deep Springs valley.

For a wave traveling in a medium with index of refraction n_1 incident on a medium with index of refraction n_2 at an incidence angle θ_i, the fraction of the incident power that is reflected (as opposed to transmitted) is determined by the Fresnel equa-

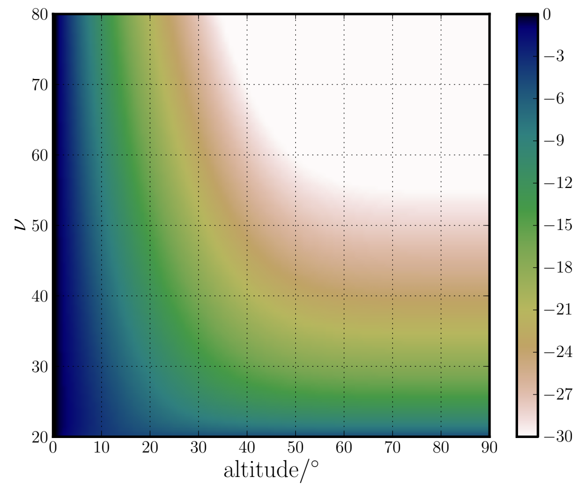

Fig. 5.— The reflectance of the ionosphere (measured in units of dB) as a function of altitude and frequency (assuming the plane-parallel approximation and $\nu_p \sim 20$ MHz).

tions. In particular, the reflectance R is given by

$$R_{TE} = \left| \frac{n_1 \cos\theta_i - n_2 \cos\theta_t}{n_1 \cos\theta_i + n_2 \cos\theta_t} \right|^2 \tag{1a}$$

$$R_{TM} = \left| \frac{n_1 \cos\theta_t - n_2 \cos\theta_i}{n_1 \cos\theta_t + n_2 \cos\theta_i} \right|^2 , \tag{1b}$$

where θ_t is the transmitted angle (determined by Snell's law), R_{TE} is the reflectance for transverse-electric waves, and R_{TM} is the reflectance for transverse-magnetic waves. For an unpolarized wave $R = (R_{TE} + R_{TM})/2$.

For waves propagating through a cold, unmagnetized plasma, the dispersion relation is $\omega^2 = \omega_p^2 + c^2k^2$. The phase velocity of these waves is ω/k so that the index of refraction is given by

$$n = \sqrt{1 + \frac{\omega_p^2}{\omega^2 - \omega_p^2}} \, . \tag{2}$$

Now restricting ourselves to the case of RFI reflecting off the ionosphere, we have $n_1 \approx 1$ and $n_2 \approx n_{\text{ionosphere}}$. $n_{\text{ionosphere}}$ is determined by Equation 2 and the fact that $\omega_p \sim 2\pi \times 20$ MHz. If we make the plane-parallel atmosphere approximation, the incident angle θ_i can be mapped to the altitude α from which the RFI appears to come from ($\alpha = 90^\circ - \theta_i$). The result of this calculation is plotted in Figure 5.

In summary, RFI above the plasma frequency can and does reflect off the ionosphere. Therefore it is probable that at least some of the RFI we are seeing at Deep Springs is generated by these reflections. Although the surrounding mountains help to block out RFI, Figure 5 shows that RFI can still sneak in through reflections.

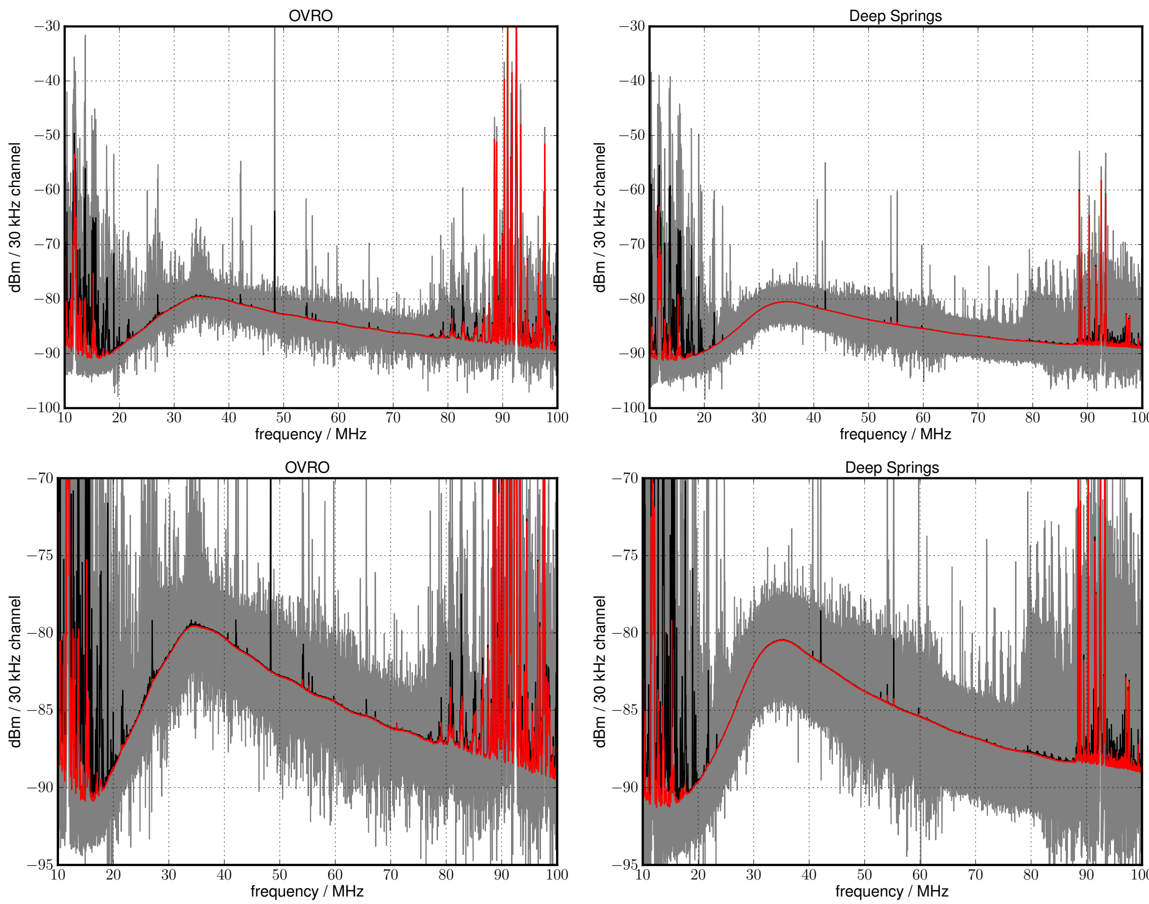

Fig. 6.— The black and red lines show the mean and medium spectra respectively over the entire observing period. The shaded gray region is bounded by the most extreme spectra such that the top of this region shows the highest power measurement at a given frequency, and the bottom of this region shows the lowest. The column on the left corresponds to measurements made at OVRO, while the column on the right corresponds to measurements made at Deep Springs. Finally, the top and bottom rows depict the same set of data with a different scale.

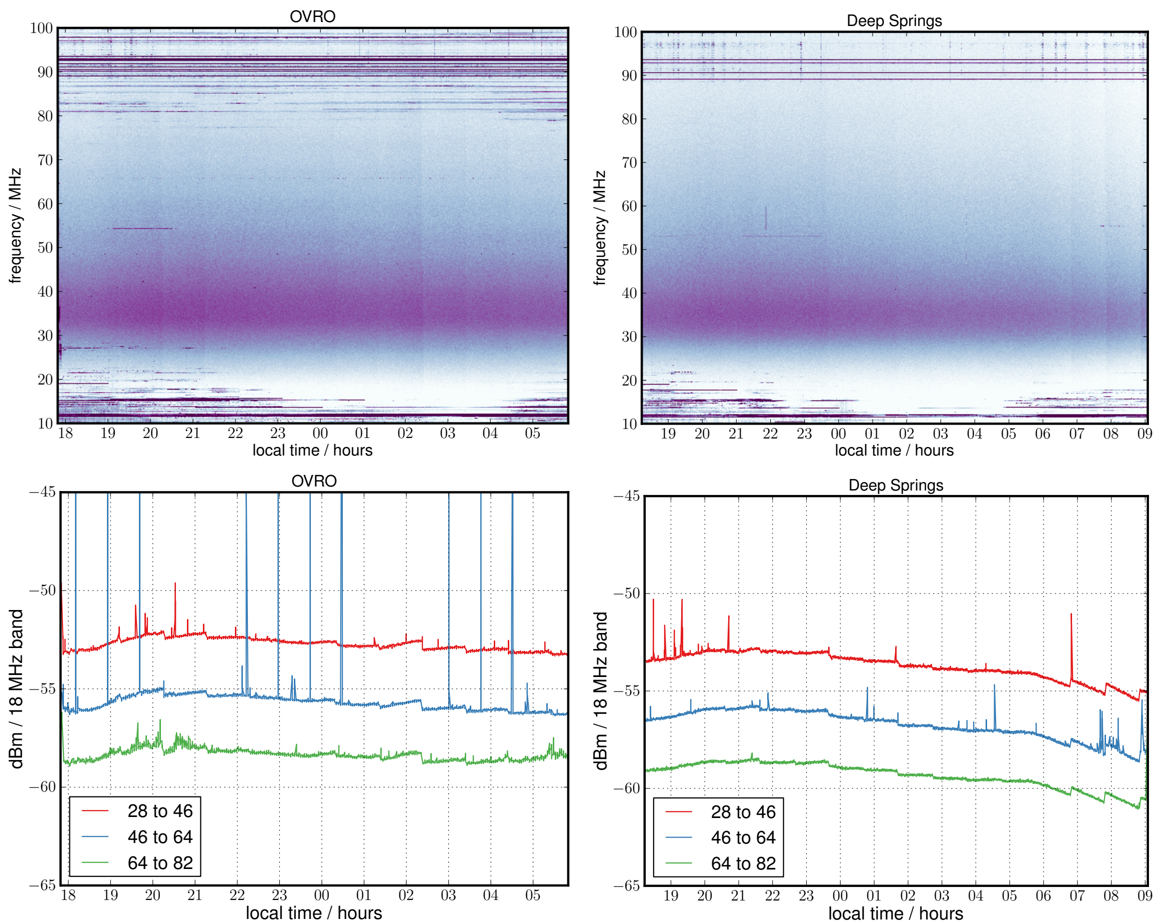

Fig. 7.— The column on the left corresponds to measurements made at OVRO, while the column on the right corresponds to measurements made at Deep Springs. The top row is a waterfall plot displaying all of the data taken at each site. Black horizontal lines are used to demarcate frequency bands. There are some barely visible vertical features in these plots, which we attribute to the spectrum analyzer periodically re-calibrating. The plots in the bottom row show the power in each frequency band as a function of time, however the 10 to 28 MHz and 82 to 100 MHz bands are omitted from the plot due to interference from the ionosphere and FM radio respectively.

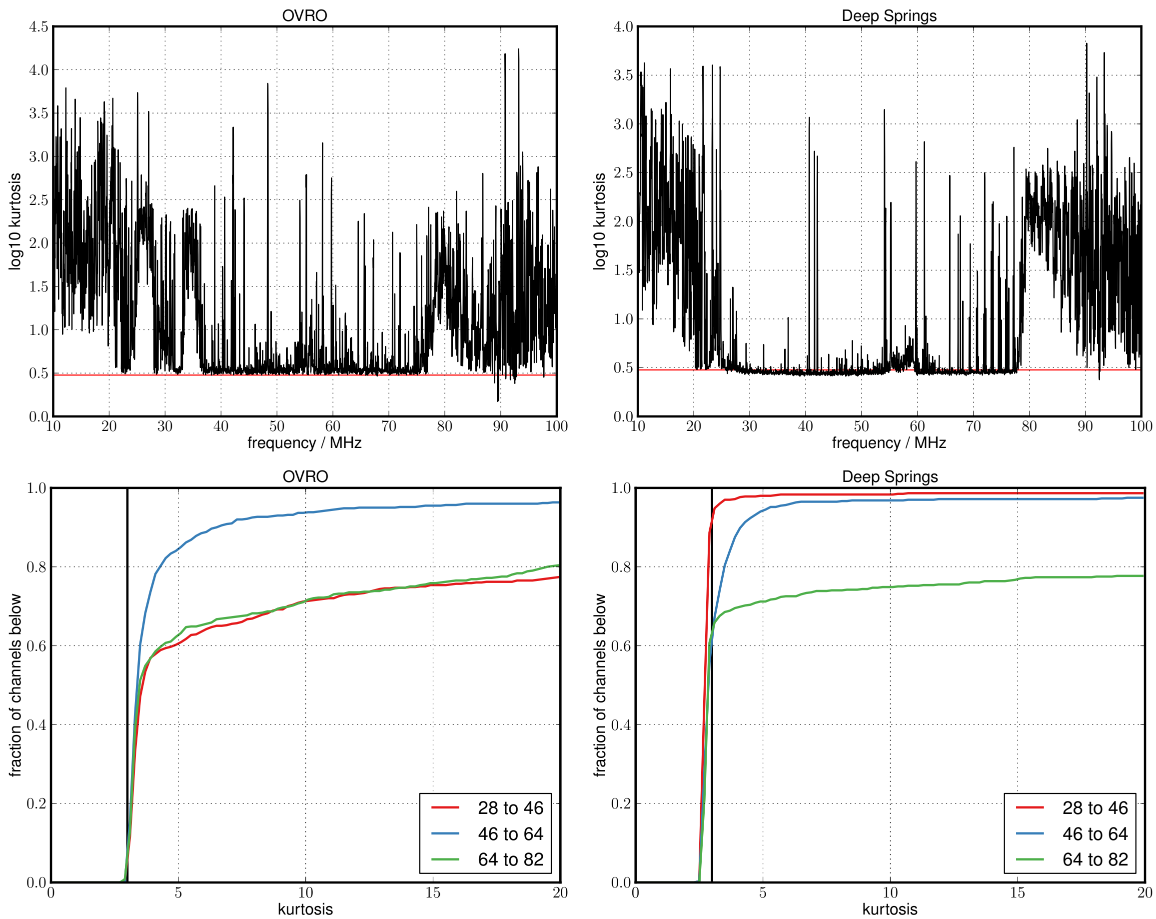

Fig. 8.— These plots characterize the kurtosis of the frequency channels at each site. Again, the column on the left corresponds to measurements made at OVRO, while the column on the right corresponds to measurements made at Deep Springs. The top row shows the kurtosis of each frequency channel measured over the entire observing period. The red line marks the value expected from a normal distribution. The bottom row shows the cumulative kurtosis distribution for three different frequency bands (that is, the fraction of channels in a given frequency range that have a kurtosis below a specific value), and the vertical black line marks the expected value from a normal distribution.

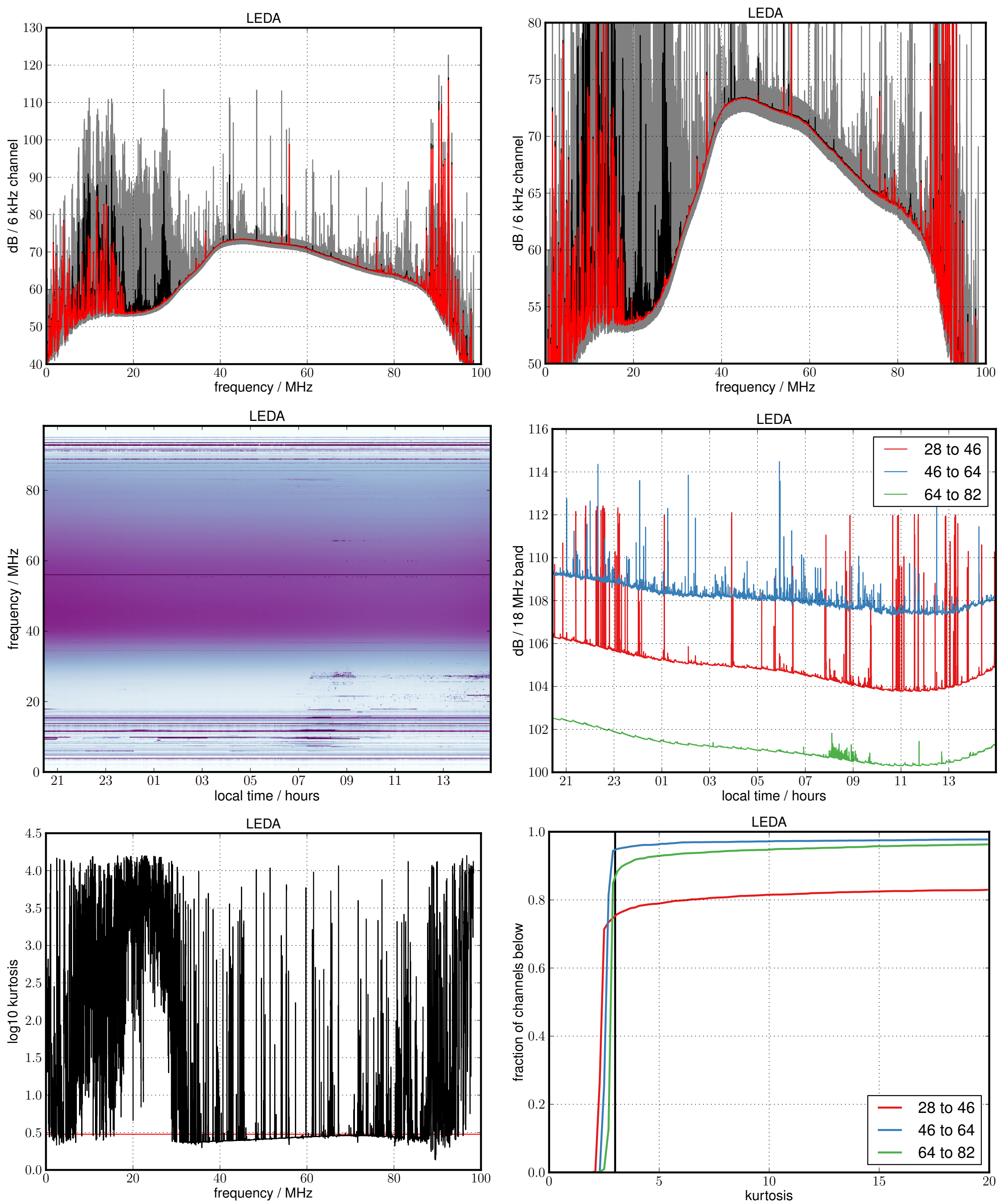

Fig. 9.— The analogous plots to Figures 6, 7, and 8 for the LEDA data.